Service and Ultimate Behavior of Adjustable Bolted Steel Plate Connections

Evan J. Gerbo, S.M.ASCE¹; Ashley P. Thrall, A.M.ASCE²; Theodore P. Zoli, P.E., M.ASCE³

3 ABSTRACT

This paper experimentally and numerically investigates the service and ultimate behavior of adjustable bolted steel plate connections: slip-critical, splice plate connections that can join wide flange sections at a range of angles as well as adjust in-situ to achieve additional angles or compensate for erection and fabrication tolerances. The connection is comprised of plates that are cold bent by press brake to a specific set of angles, forming a prefabricated, kit-of-parts. Adjustability is achieved by further cold bending the plates in the field through bolt tightening. The slip and bolt shear behavior of the connection was experimentally tested by applying an axial force on a wide 10 flange member (via a servo-controlled hydraulic actuator in displacement control) joined by the 11 tested connection to another wide flange member (restrained by a rigid reaction frame). A total of 12 18 scenarios were tested to investigate the effect of (1) direction and amount of cold bend via bolt 13 tightening, (2) tightening approaches, (3) direction of loading, and (4) plate and member angle on behavior. A finite element numerical modeling approach was developed and validated, offering 15 additional understanding of bolt behavior in the adjustable bolted steel connection. A degradation in slip capacity was observed due to a reduced clamping load. During bolt tightening, the bolts deform non-flush plies into contact with the flanges and are simultaneously being bent by contact with the plates, leading to this reduced clamping load. The bolt shear capacity can also be degraded due to the connection geometry which can reduce the engagement of shear planes. Recommendations for reductions in slip and bolt shear capacity are developed. Importantly, findings also offer

¹PhD Candidate, Kinetic Structures Laboratory, Department of Civil & Environmental Engineering & Earth Sciences, University of Notre Dame, Notre Dame, IN 46556. E-mail: egerbo@nd.edu

²Myron and Rosemary Noble Associate Professor of Structural Engineering, Kinetic Structures Laboratory, Department of Civil & Environmental Engineering & Earth Sciences, University of Notre Dame, Notre Dame, IN 46556. (corresponding author) E-mail: athrall@nd.edu

³National Bridge Chief Engineer, HNTB Corp., Empire State Building, 350 5th Ave., 57th Floor, New York, NY 10118. E-mail: tzoli@hntb.com

- insight into the behavior of bent connections, as well as misaligned or non-flush connections that are force-fit in the field.
- Author Keywords: Bolted steel connection; Slip-critical connection; Cold bending; Prefabrication; Rapid erection; Misaligned connection; Force-fitting

6 INTRODUCTION

Adjustable bolted steel plate connections [Figure 1, introduced in Gerbo et al. (2018) and 27 Gerbo et al. (2019a)] are a kit-of-parts approach to join angled structural members through cold bending. Specifically, bent flange splice plates join flanges of wide flange sections in double 29 shear. It is envisioned that webs would also be joined in double shear using straight and flush 30 splice plates. The resulting slip-critical connection is moment-resisting as the webs and flanges 31 are joined independently. The bent flange plates are a prefabricated, kit-of-parts which are prebent 32 to prescribed angles ($\gamma = 5$, 10, 15 degrees, or a 0 degree non-bent plate) through cold bending 33 via a press brake (Figure 1A). To join members at a wider range of angles, α or to adjust for 34 erection and fabrication tolerances, the prebent flange plates can be further cold bent via bolt 35 tightening during installation (Figure 1C, D), i.e., bolts deform the non-flush plies (with difference in ply angle $\delta = \alpha - \gamma$) to contact with the flange. In this way, the prefabricated, kit-of-parts can be used for many connections within one structure or among different structures, leading to 38 construction cost and time savings through mass production of connection details. The adjustable bolted steel plate connection is intended for connections between any two angled wide flange members. Applications include both buildings (for example for the apex connections of portal frames) and bridges (for example for angled connections in arches or trusses).

In prior research, the authors have (1) experimentally and numerically investigated the strains induced in the plates due to prefabrication via press brake (Gerbo et al., 2016), and (2) experimentally and numerically investigated the plate and bolt strains due to installation via bolt tightening (Gerbo et al., 2018, 2019a,b). However, there is a major research gap in understanding the effect of the installation process and the connection geometry on the service (or slip) and ultimate behavior of these connections. During field installation, the bolts plastically deform the non-flush plates, are

in eccentric contact with the non-flush plates, and are bent by contact with the plates, all resulting in degradation of the slip load. The peak bolt shear load can also be affected as the connection geometry can result in shear planes not being fully engaged or not in contact.

This research has wider relevance in steel design, fabrication, and construction, specifically for 52 bent plates in skewed or kinked connections, as well as misaligned or non-flush connections. The 53 use of bent plate connections is commonplace in skewed and curved girder cross frame connections 54 for bridges and skewed beam connections in buildings. Bent plate connections between piecewise 55 straight components are also emerging as a cost-effective alternative to fabricating curved beams or 56 girders. Additionally, connections that are designed and fabricated as straight may be misaligned 57 in the field due to poor fit up. Force fitting of these connections can induce unanticipated forces and/or distortion in these connections. How much misalignment and distortion can be tolerated, and its effect on service and ultimate behavior is an important consideration in structural steel design and detailing. Performance issues associated with plate contact, bolt hole geometry, bolt 61 flexure, and forces induced during bolt up are often issues with these types of connections. While the behavior of slip-critical, straight and flush splice connections is well understood (Kulak et al., 63 2001), the performance of bent and misaligned or non-flush connections has received comparatively little attention. The research presented in this paper is an important first step in developing a comprehensive understanding of behavior of these bent and misaligned or non-flush and their associated design implications. 67

This paper is the first investigation of the service and ultimate behavior of adjustable bolted steel plate connections and the more general case of bent connections, as well as misaligned or non-flush connections. The focus is on understanding slip behavior and the failure mode of bolt shear.

OBJECTIVES AND SCOPE

The objective of this paper is to understand the service and ultimate behavior of adjustable bolted steel plate connections. A total of 18 connection scenarios were experimentally tested to failure under axial force at approximately 1/3 scale to understand the effect of (1) direction and

amount of cold bend via bolt tightening (Scenarios 3-5), (2) tightening approaches (Scenarios 6,7), (3) direction of loading (Scenario 8), and (4) plate and member angle (Scenario 9-16) (Figure 2, Table 1). Scenario 3 was a benchmark case that was tested 3 times to demonstrate repeatability. The plates for each tested scenario were first prebent via press brake and then installed [fol-79 lowing the installation procedures recommended by Gerbo et al. (2018) and Gerbo et al. (2019a)] to join two wide flange members in a rigid reaction frame. A servo-controlled hydraulic actuator 81 in displacement control was then used to load the connection to failure via bolt shearing. As this 82 is the first investigation on the service and ultimate behavior of the adjustable bolted steel plate 83 connection, this study focused on the axial tension behavior of the connection, with the actuator 84 aligned concentrically with one of the joined wide flange members. The bolt shear failure mode 85 was investigated as the installation process induces bending in the bolts which can impact bolt per-86 formance. Scenario 8, with a large gap between members, was tested in compression. However, 87 it is envisioned that the plates and gap between members would be appropriately dimensioned to avoid the failure mode of plate buckling when loaded in compression. Throughout testing, the load, actuator displacement, relative movement (or slip) of plates, plate surface strains, and residual bolt 90 surface strains were measured. 91

The measured data are compared to finite element (FE) numerical modeling, resulting in a validated FE numerical modeling approach and providing further insight into bolt behavior. Recommendations for reductions in slip and bolt shear capacity are developed. Research results are relevant to the behavior of bent connections, as well as misaligned or non-flush connections that are force-fit in the field. Measured behavior of straight and flush control specimens provides further insight into slip-critical connections in general.

EXPERIMENTAL PROGRAM

Tests were performed at approximately 1/3 scale, due to laboratory limitations. All components, including the bolts, plates, and members, were scaled to ensure that the strain distributions would be similar to full-scale connections. It is acknowledged that there are scaling effects related to bolt size and clamping pressure. However, experiments would be able to capture the general

service and ultimate behavior of the connection. Each scenario used 4.76 mm (0.188 in.) thick ASTM A36 steel plates joined the flanges of W4x13 wide flange members in double shear. Three 104 plates joined the top flanges (T) and three plates joined the bottom flanges (B). Single 88.9 mm 105 (3.50 in.) wide outer (O) plates and two 31.8 mm (1.25 in.) wide inner (I) plates straddled the web 106 connecting each flange. All plates were 152 mm (6.00 in.) long [except for Scenario 8 which are 107 212 mm (8.33 in.) long]. The plates were joined to each flange by 8, 6.35 mm (0.250 in.) diameter 108 SAE Grade 5 (SAE, 2014) bolts [equivalent mechanical properties and similar chemical properties 109 to ASTM A325 (ASTM, 2014a) bolts]. Two ASTM F436 (ASTM, 2018) washers were used with 110 each bolt, along with Grade A nuts. With the exception of Scenario 2 which used standard size 111 holes [7.14 mm (0.281 in.) diameter] in the plates and flanges, the flanges had long slots [7.14 mm 112 x 15.9 mm (9/32 in. x 5/8 in.)] and the plates had oversized holes [7.94 mm (5/16 in.)]. As the 113 connection was approximately 1/3 scale, the scaled oversized hole diameter was targeted to be 1/3 114 of the typical 3.18 mm (1/8 in.) larger than bolt diameter. This was rounded to the nearest available 115 drill bit size of 7.94 mm (5/16 in.). The long slots and oversized holes were selected to create a 116 versatile kit-of-parts with few number of unique components (Gerbo et al., 2018). Scenario 1 was 117 a straight and flush control specimen, with the same hole geometry as the adjustable bolted splice 118 plate connection (Figure 2A-C). Scenario 2 was also a straight and flush control specimen, but with 119 plates and flanges having standard size holes.

Prior to testing, the plates were prebent via press brake with a 38.1 mm (1.50 in.) radius to angles, γ (Figure 1A). The radius is equivalent to $8t_s$, where t_s is the thickness of the plates. This was selected as it exceeds the $5t_s$ minimum radius prescribed by recent revisions to bridge design code (AASHTO, 2012).

The prebent plates were then installed via bolt tightening to join the two W4x13 members following the procedures recommended in Gerbo et al. (2018) and Gerbo et al. (2019a). The plates and bolts were first loosely assembled on the W4x13 members, with assemblies adjusted to have approximately the same starting position position. The nuts and washers were initially assembled by hand, with the distance from the tip of the bolt to the face of the nut equalized among the bolts

to within 0.254 mm (0.01 in) to ensure a symmetric starting position. Bolt tightening was then performed using a torque wrench. Tightening was performed in a criss-cross type pattern, pro-131 gressing from bolt 1 through bolt 8 (Figure 1E-F), with 1 turn occurring per increment until firm 132 contact was achieved between plates and flanges at all bolt locations [firm contact was defined by 133 no longer being able to fit a 0.0762 mm (0.00300 in.) shim between the plates and flanges]. An 134 additional 5/6 turn of each bolt was then performed as an adaptation of the turn-of-nut criteria (Re-135 search Council on Structural Connections, 2014). During installation, one W4x13 was supported 136 by a rigid reaction frame (with top and bottom flanges, as well as the web, bolted to the frame) and 137 the other was supported by a stub column (bottom flanges were bolted to the stub column, Figure 138 2A,D). The stub column was removed prior to testing the connection to failure. 139

Testing was then performed on the installed connection by applying an axial force on the 140 W4x13 member [moving member (M), hereafter], previously secured to the stub column, using a 141 servo-controlled hydraulic actuator [Parker 0.500 BB2HT14A 6.500, 20.7 MPa (3000 psi), 262 kN 142 (58.9 kips) capacity] in displacement control, at a rate of 0.457 mm/min. (0.0180 in./min.) (Figure 143 2B-C,E-F,G). The other W4x13 member [static member (S), hereafter] remained restrained to the 144 reaction frame. All tests were performed in tension, with the exception of Scenario 8 which was in 145 compression. Testing continued for each scenario until bolt failure or 50% drop in load (in the case 146 of Scenario 8). The self-reacting reaction frame was modular, with different positions for member and hydraulic actuator to accommodate the tested scenarios. The focus of the research was on the 148 behavior of the flange plates and bolts. Therefore, no web splice plates were used.

Figure 2H-I shows the instrumentation. Displacements were measured using string potentiometers (MD Totco 1850-002) and linear potentiometers (BEI 9615R5.1KL2.0). A linear potentiometer (Balluff BTL6-A500-M0178-PF-S115) attached to the hydraulic actuator measured the actuator displacement. Pressure transducers (Anfield TG-300P-G-3-M12-4MA3, 3000 psi) measured the force in the actuator. The TO and BO plate surface strains due to prebending via a press brake, installation via bolt tightening, and loading to failure were measured using the photographic measurement technique three-dimensional (3D) digital image correlation [DIC, see Gerbo et al.

(2016), Gerbo et al. (2018), and Gerbo et al. (2019a)]. An assembly of mirrors facilitated the DIC measurements (Figure 2I). DIC was also used to measure the residual strains in the bolts.

The instrumentation confirmed that the self-reacting reaction frame had negligible deformation during testing [less than 1.27 mm (0.05 in.)]. The static member elastically displaced relative to the reaction frame, as measured by the string potentiometers. In the actuator force, F versus actuator displacement, Δ plots, this elastic displacement was removed by projection along the actuator axis.

163 MATERIAL PROPERTIES

Table 2 provides the measured material properties of the ASTM A36 (ASTM, 2014b) plates 164 and the SAE Grade 5 (SAE, 2014) bolts used in the experimental tests. ASTM material testing of 165 the plates was performed using an Instron 5590 Universal Testing Machine (ASTM, 2017b,a,c,d). 166 A total of 5, full thickness [4.76 mm (0.188 in.)] samples (all from the same bar) were tested, ac-167 cording to the required ASTM dimensions (ASTM, 2017a) for a 50.8 mm (2 in.) gauge length. The 168 tensile testing was performed in the same direction as the final direction of rolling of the samples 169 (ASTM, 2017b). This corresponds to the longitudinal axis of the connection (Figure 1). ASTM 170 material testing of 5 bolts was performed by Laboratory Testing, Inc. (Hatfield, Pennsylvania) 171 according to ASTM standards (ASTM, 2016).

173 NUMERICAL MODELING

3D FE numerical analyses of the connection behavior were performed in ABAQUS Standard (ABAQUS, 2014), using C3D8R solid elements with a typical mesh size of 1.02 mm (0.04 in.) in the plates, 0.508 mm (0.02 in.) in the bolts, and 2.54 mm (0.1 in.) in the wide flange members. Nonlinear material models with isotropic hardening were used for the plate and bolts, based on the measured stress-strain behavior (Table 2). Geometric nonlinearity was also used.

Symmetry about the longitudinal direction was employed to reduce computational expense (Figure 3). Boundary conditions to enforce symmetry included translation restraints in the xdirection along the longitudinal centerline of the connection. Boundary conditions to simulate the
self-reacting frame included translation restraints in all 3 directions along the truncated face of the

static member. During bolt installation, the truncated face of the moving member has the same restraints. The bolt tightening process was simulated using the approach developed and validated in Gerbo et al. (2019a). After bolt installation, the restraints on the truncated face of the moving member were removed, allowing the connection to elastically spring back (simulating removal of the stub column). The actuator was simulated using a slot-type connector to induce displacements while allowing in plane rotation at each end of the actuator.

To include the effect of residual strains and strain hardening from prefabrication via press brake, the bending process was first modeled using the approach developed and validated in Gerbo et al. (2016).

BEHAVIOR OF STRAIGHT AND FLUSH BOLTED SPLICE CONNECTIONS

Figure 4 shows the actuator force, F versus actuator displacement, Δ for the two straight and 193 flush scenarios, with slip and peak load provided in Table 1. Scenario 1 had a 15.5% higher 194 measured load at slip initiation compared to Scenario 2. This can be attributed to "caving" of 195 the plates into the longs slots in the flanges, increasing frictional resistance. The initiation of slip 196 and its location is identified by a marker. As expected, the slip plateau of Scenario 1 was much 197 longer than Scenario 2 due to the additional play provided by the long slots. Both Scenario 1 and 198 2 reached similar peak loads, with Scenario 1 being just 3.36% higher, demonstrating that the hole 199 size did not impact peak load. 200

201 Closed-Form Design Code Predictions

192

Current design code (AISC, 2017) predicts slip capacity, ϕR_{n-Slip} for straight splice connections as:

$$\phi R_{n-Slip} = \phi \mu D_u h_f T_b n_s n_b \tag{1}$$

where ϕ is a factor considering hole size [1 for standard holes, 0.7 for long slots (in this paper, comparisons use the 0.7 value for consistency, even though Scenario 2 should use 1.0), μ is the mean slip coefficient (0.30 for Class A surfaces), D_u is a multiplier reflecting the ratio of mean installed bolt pretension to the specified minimum bolt pretension (1.13), h_f is a factor for fillers

(1.0 for no fillers), T_b is the minimum fastener tension force, n_s is the number of slip or shear planes per bolt (2), and n_b is the number of bolts (4). T_b is typically provided in design code (AISC, 2017), but the size of the bolts in this research were smaller than those provided in the code. Instead, T_b is calculated per the recommendation of AISC (2017) as:

$$T_b = 0.70F_t A_s \tag{2}$$

where F_t is the minimum specified tensile strength [830 MPa (120 ksi), (SAE, 2014)], and A_s is the stress area in metric units (ASTM, 2015):

$$A_s = 0.7854[D - (0.9382P)]^2 (3)$$

where D is the bolt diameter [6.35 mm (0.250 in.)] and P is the thread pitch [1.27 mm (0.05 in.)]. Therefore, $\phi R_{n-Slip} = 23.0$ kN (5.16 kips) for long slots and $\phi R_{n-Slip} = 32.8$ kN (7.37 kips) for standard holes.

Using these predictive equations, Scenario 2 should actually have a higher slip load than Scenario 1. The measured slip load of Scenario 2 does not even achieve the design code prediction. This sample size is too small to make recommendations related to this difference, but it indicates an area for future research. The measured slip load for Scenario 1 exceeded the predicted slip load (using ϕ =0.7).

The predicted bolt shear capacity, $\phi R_{n-Shear}$ from current design code (AISC, 2017) is:

$$\phi R_{n-Shear} = \phi F_{nv} A_b n_s n_b \tag{4}$$

where ϕ is a reduction factor (0.75), F_{nv} is the nominal shear stress of the bolt [469 MPa (68 ksi), (AISC, 2017)], and A_b is the nominal area of the bolt [31.7 mm² (0.0491 in.²)]. Both single (subscript 1) and double shear (subscript 2) are compared in this paper with $\phi R_{n-Shear-1} = 44.6$ kN (10.1 kips) and $\phi R_{n-Shear-2} = 89.2$ kN (20.1 kips). Scenario 1 and 2 both exceed this design

code prediction.

BEHAVIOR OF ADJUSTABLE BOLTED STEEL PLATE CONNECTION

Figure 4 also compares the measured force-displacement behavior of the benchmark adjustable bolted steel plate connection (Scenario 3) with the two straight and flush control specimens.

The benchmark Scenario 3 was tested three times to demonstrate repeatability. Among the 231 three tests, the measured slip load varied up to 21.5% compared to the average measured value of 232 12.4 kN (2.79 kips). The measured peak load varied just 4.98% compared to the average measured 233 value of 90.3 kN (20.3 kips). The higher variability of the slip load can be attributed to differences 234 in surface roughness. All three tests had slip initiate at a bottom flange faying surface, with the 235 final slip occurring at a top flange faying surface. The length of the measured slip plateau and 236 the displacement at peak load were similar among the three tested scenarios [varying up to 4.80%] 237 compared to the average of 12.7 mm (0.500 in.)]. 238

239 Comparison to Straight and Flush Connections and Closed-Form Design Code Predictions

Scenario 3 tests had an average reduction in measured slip load of 57.3% compared to Scenario 1. While Scenario 1 exceeded the predicted slip load, ϕR_{n-Slip} (with $\phi=0.7$) by 26.4%, the average measured slip load for Scenario 3 was 46.1% below ϕR_{n-Slip} . These tests also had a reduced measured peak load, averaging 41.3% less than Scenario 1 and just 1.42% more than the predicted double shear capacity, $\phi R_{n-Shear-2}$.

245 Mechanics Based Understanding of Behavior

Compared to a straight and flush scenario, the bolts of adjustable bolted steel plate connections:

(1) need to deform non-flush plates to contact with flanges (overcoming the difference in ply angle, δ), hereafter δ -effect (Figure 5A) and (2) are bent by contact with the plates (oversized plate holes

and long slots in the flanges enable a bolt to fit through all three plies prior to bolt tightening,

but the bolt will be deformed flexurally through plate contact during tightening, Figure 5B-C),

hereafter interference-effect. In the δ -effect, the additional force needed to bring non-flush plies

together reduces clamping load of the bolts (Figure 5A). Further, as the bolts are in eccentric

contact with the initially non-flush plies, flexure also occurs, further degrading the clamping load. These mechanisms degrade the clamping load, reducing the slip capacity of the connection. This 254 δ -effect only occurs in scenarios for non-zero δ . In the interference-effect, bending in the bolts 255 causes plate contact during bolt installation resulting in friction between the bolt shank and edge 256 of the plate holes (F_n in Figure 5B), reducing the clamping load along the bolt axis. The catenary 257 action in the bolt redirecting the bolt pretension around the corner of the plate hole edge results in 258 further frictional losses (F_c in Figure 5C). These mechanisms also degrade clamping load, reducing 259 the slip capacity. This interference-effect only occurs when the bolts contact the plates during 260 installation. The δ -effect and the interference-effect induce flexure in the bolts, contributing also 261 to a reduction in bolt shear capacity. Both of these effects could occur for the more general case of 262 bent connections, as well as non-flush (related to the δ -effect) or misaligned (where holes are not 263 aligned, related to the interference-effect) connections. Force fitting is typically performed on non-264 flush or misaligned connections, but reductions in capacity from force fitting are not considered in 265 design. 266

An analytical indicator of the interference-effect is the metric e_b [Figure 5C, first developed in Gerbo et al. (2019a)] which is an approximation of the amount of bolt deformation due to plate contact occurring during installation. This e_b metric is calculated as:

$$e_b = e_h - (d_{ph} - d_b) \tag{5}$$

where e_h is the offset between the plate holes (Figure 5D), calculated as:

$$e_h = |(t_m + t_s) \tan \alpha| + \frac{e_d}{\cos \alpha} \tag{6}$$

where t_m is the thickness of the flange, t_s is the thickness of the plates, d_{ph} is the plate hole

diameter, d_b is the diameter of the bolt, and e_d is determined as follows:

$$e_{d} = \begin{cases} l_{\delta 1}(\cos \gamma - \cos \alpha) & \text{if } \delta \ge 0 \\ g(\cos \gamma - \cos \alpha) & \text{if } \delta < 0 \end{cases}$$
 (7)

where $l_{\delta 1}$ is the distance from flange edge to the center of its hole and g is the gap between 273 wide flange members (Figure 1C). Note that negative or zero values of e_b indicate that there is 274 no interference-effect. 275

The reduced measured slip load of Scenario 3, with $\delta=2.5^{\circ}$ and one of the highest value 276 of e_b in the experimental testing program (Table 1), can be attributed to both the δ -effect and the 277 interference effect. 278

The adjustable bolted steel plate connection is intended to be in double shear for economy in 279 number of fasteners. However, depending on the offset between the plate holes, e_h only the shear plane towards the convex side of the connection may be fully engaged, with the other partially engaged or not at all (Figure 5D). This is due to the holes in the plates having identical locations in 282 the prebent state. This partial engagement of one of the shear planes was evident in the deformed 283 shape, measured via DIC, of an example bolt from Scenario 3a compared to one from Scenario 284 1 in which both shear planes are engaged (Figure 6A). Figure 6B shows the location of the bolt 285 centerline (based on measured DIC data) for all bolts in Scenario 1 and 3a. As the bolt centerline 286 crosses the shear planes, full shear engagement would be indicated by a vertical jump in the cen-287 terline. Figure 6B shows that occurs for all shear planes of Scenario 1, indicating full double shear 288 behavior. Scenario 3a shows engagement at a single shear plane, indicating single shear behavior. 289

Effect of Direction and Amount of Cold Bend via Bolt Tightening

281

290

To investigate the effect of direction $(\pm \delta)$ and amount $(|\delta| = 0^{\circ} \text{ or } 2.5^{\circ})$ of cold bending via 291 bolt tightening while maintaining a constant member angle $\alpha = 12.5^{\circ}$, Scenario 5 ($\delta = -2.5^{\circ}$) is 292 compared with Scenario 3 ($\delta = 2.5^{\circ}$) and a flush Scenario 4 ($\delta = 0^{\circ}$) in Figure 4. 293

Notably, the flush and $-\delta$ scenarios had similar slip loads [15.9 kN (3.57 kips) and 16.6 kN 294 (3.74 kips), respectively], which were 45.9% and 48.1% higher than the average of the bench-295

mark Scenario 3 tests. While the slip loads for flush and $-\delta$ scenarios are higher than benchmark Scenario 3, they are 45.2% and 42.6% lower, respectively than Scenario 1.

298

299

300

301

302

303

304

305

306

307

308

309

310

311

312

313

316

317

318

319

320

321

322

The higher slip load for the flush scenario can be attributed to the lack of δ -effect and a reduced interference-effect as Scenario 4 has a lower value of e_b . In the $-\delta$ scenario, there was a δ -effect, but it was reduced as the plates were being bent in the opposite direction compared to prefabrication via press brake. As a result of the Bauschinger effect, their yield strength in the direction of field bending via bolt tightening would be reduced, thereby reducing the amount of force required to bring the plies into contact. The interference-effect was also reduced due to a lower e_b .

The direction and amount of δ also impacted the progression of slip. Figure 7 shows the slip of each faying surface as a function of actuator displacement, Δ . The measurements at inner pairs of plates generally agree with each other, and were therefore averaged for simplicity. Straight and flush Scenario 1 showed that the plies of the top flanges and bottom flanges slipped nearly simultaneously, as expected. In contrast, all plies of the bottom flange of Scenario 3a slipped prior to the plies of the top flange. The flush Scenario 4 showed similar behavior to Scenario 3a, with the bottom flanges slipping before the top flanges. This was because there was still a slight preference to slip the bottom flange first due to the bent portion of the plate contacting the edges of the member flanges. The $-\delta$ Scenario 5 had near simultaneous slip of the top and bottom flanges. This was due to the elastic strains induced in the plates during installation via bolt tightening and the location of plate contact. Specifically, the elastic strains from installation spring the connection back towards the initial plate angle. In $+\delta$ scenarios this results in the top flange being preloaded in compression, and the bottom flange being preloaded in tension. When tensile loads were then applied, the bottom flange slipped first. The contact location between plates and the flange resulted in additional stored elastic energy for a similar springback effect. The springback effect from $-\delta$, though it would be in the opposite direction, would be less in magnitude due to the Bauschinger effect. This scenario also did not have the same plate contact location which causes the preference toward bottom flange slip.

The direction and amount of cold bending via bolt tightening did not substantially influence the

peak loads. All 3 scenarios, which have similar e_h values, do not achieve shear capacities similar to Scenario 1, indicating that only one shear plane was being fully engaged.

Effect of Varying Tightening Approaches

325

Two alternative bolt tightening approaches were investigated: (1) Scenario 6 using beveled washers and (2) Scenario 7 where additional tightening was applied to each bolt.

As there was an observed reduction in slip and peak load in the adjustable bolted steel plate 328 connection, Scenario 6 investigated the use of beveled washers to reduce the effect of eccentric 329 contact at the bolt head and nut due to the difference in ply angle δ . The angle of the bevel was 330 2.5°, matching the magnitude of δ . Scenario 6 had a 49.1% lower slip load and a 12.9% lower peak 331 load than the comparable Scenario 3. Beveled washers create directionality to the bolt pretension which precipitates slip in a particular direction at low loads. The reduction in ultimate load was 333 a result of the bolts being angled relative to the plates (as opposed to perpendicular to the plates) 334 in the final tightened position. This places the bolts even more into a single shear environment as 335 opposed to double shear. Beveled washers are therefore not recommended. Indeed, the bottom 336 plies of the static member actually slipped during the removal of the stub column. 337

In Scenario 7, the tightening procedure was altered to consider firm contact when not only 338 the plates have contacted the flange, but also the bolt head and nut were in firm contact with the 339 washers. This resulted in an extra 1/2 turn. This increased tightening was investigated as a potential 340 means of compensating for the observed loss in slip capacity. Bolt 6 on the bottom flange of the 341 static member broke during installation, indicating that too much bolt pretension was applied. 342 While 5 of the bolts were able to be tightened to this amount, the torque required to tighten the 343 nuts started to decrease towards the end of tightening, indicating that the bolts were close to failure. 344 This increased bolt tightening is not recommended. 345

346 Effect of Direction of Loading

Scenario 8 was tested in compression. A larger gap, g between the members [63.5 mm (2.50 in.)] was used as the gap for all other scenarios [4.24 mm (0.167 in.)] would have resulted in bearing of the members after partial slip. Figure 8 shows the force-displacement curve for Scenario

8 compared to Scenario 3a, both with the same member and plate angles. The slip load for Scenario 8 was just 1.6% higher than the average of Scenarios 3a, 3b, and 3c, indicating no change to the slip 351 load. Scenario 8 had slip initiate at the top flange first as opposed to the bottom flange in Scenario 3. 352 This was because of the internal stresses developed during the installation process, which attempt to 353 spring the connection back towards the initial plate angles, as discussed earlier. For $+\delta$ scenarios, 354 the elastic springback preloads the top flange in compression, causing it to slip before the bottom 355 flange when loaded in compression. The peak load in Scenario 8 was significantly reduced. This 356 was expected as an angled or bent connection (i.e., member angle, α) was placed in compression 357 as opposed to tension. Failure was defined as 50% drop in load. No bolts were broken. 358

Effect of Varying Plate and Member Angles

359

364

365

366

367

368

369

The kit-of-parts for the adjustable bolted steel plate connections is comprised of plates with initial angles $\gamma=0,5,10,15^{\circ}$. These connection plates were tested at varying member angles, α with varying differences in initial ply angle, δ . Figure 9 shows the force-displacement curves corresponding to each of these scenarios, demonstrating experimental evidence of behavior.

The slip and ultimate behavior of this kit-of-parts are compared with the behavior of the other tested scenarios in Figure 10 and Figure 11, respectively. The measured force F (with susbscript s for slip force and p for peak force) is normalized with respect to the closed-form design predictions, where a value above 1 indicates conservatism and below 1 indicates unconservatism. The horizontal axis indicates the metrics e_b and e_h , normalized with respect to the bolt diameter d_b . The markers correspond to the scenario number.

Figure 10 shows the impact of the δ -effect and the interference-effect (measured by e_b , with negative e_b indicating no interference) on the measured slip load. Flush Scenario 10, as well as the straight and flush control Scenario 1 and 2, have no δ - or interference-effects and have comparable slip loads. Scenario 9 and 12, for which there was only the δ -effect, show slightly reduced slip loads, but all are still conservative with respect to the design code predictions. In contrast, Scenarios 13, 4, and 15 only have the interference-effect. Scenarios 13, 4 and 15 show significant degradation of slip load and demonstrate that the design code predictions are unconservative when

bolts are bent by plate contact during installation. Comparing the impact of the δ -effect to the interference-effect, the interference-effect dominates behavior. For scenarios with both the δ - and 378 interference-effects, there is a trend of decreasing measured slip load with increasing e_b/d_b 379

Figure 11 investigates the peak load of the scenarios, compared with the analytical approxi-380 mation for the offset between the plate holes, e_h . e_h/d_b is compared with the required minimum 381 elongation for the relevant bolt standard [in this case 14%, (SAE, 2014)]. If e_h/d_b is less than the 382 minimum elongation strain, this ensures that the bolt can sufficiently deform, without rupture, to 383 engage the lagging shear plane. The measured amount of shear plane deformation, s is investi-384 gated in Figure 12. s is calculated by taking the difference in the measured lateral location of the 385 centerline of the deformed bolt across a shear plane and normalizing by the bolt diameter (e.g., 386 Figure 6B). A zero value indicates no shear. Larger values indicate increased shear deformation, 387 with a peak possible value 0.237 based on the measured rupture strains from tensile testing. 388

Scenarios 1, 2, 9, and 12 all have large values of s at both shear planes, indicating full shear 389 engagement. The measured peak load of these scenarios in Figure 11 also indicates double shear behavior. This confirms that the limit that e_h/d_b be less than the minimum elongation strain ensures double shear behavior. Indeed, Scenarios 1, 2, 9, and 12 all have peak loads far exceeding the design code prediction for double shear.

390

391

392

393

For scenarios with e_h/d_b greater than the required elongation, both shear planes are not fully 394 engaged. Figure 12 shows that with increasing e_h/d_b , s decreases for the shear plane near the head 395 (for the top flange bolts) or the shear plane near the tip (for the bottom flange bolts), indicating 396 lack of engagement. For these cases with e_h/d_b greater than the required elongation, the measured 397 peak load was reduced. A designer could conservatively design these scenarios assuming single 398 shear behavior. 399

Data is not shown for Scenario 16 as a bolt broke during installation. e_b/d_b values should be 400 kept below 0.5, as this was found to rupture bolts in Scenario 16. 401

Numerical Predictions

The FE numerical model for Scenario 3 predicted a slip load of 14.0 kN (3.14 kips), 12.9% higher than the average measured slip load from the Scenario 3 tests (Figure 10). The predicted peak load was 98.3 kN (22.1 kips), just 8.66% higher than the average measured value (Figure 11). In comparison, the FE numerical model for straight and flush Scenario 1 predicted a slip load of 52.5 kN (11.8 kips), 81.0% higher than the measured slip load and a peak load of 173 kN (39.0 kips), 12.3% higher than the measured peak load.

Generally, the FE models were able to more closely predict the peak load compared to the 409 slip load for both Scenario 1 and Scenario 3. The slip load prediction is highly dependent on 410 the frictional coefficient between the plies and the amount of applied clamping load. In the FE models, a frictional coefficient of 0.33 was assumed as recommended for steel-on-steel faying 412 surfaces (Kulak et al., 2001; AASHTO, 2014). In reality, the frictional coefficient may have been 413 different and may have varyied among the faying surfaces. In the FE models, the applied clamping load via bolt tightening was simulated by an induced displacement. This does not capture the 415 combined stress state of torsion and tension while tightening the bolt. Indeed, it was observed that 416 the bolt tips rotated 25 degrees, on average for all scenarios, relative to the head during tightening. 417 This difference may have impacted the clamping load. Differences in the prediction of the peak 418 load can be attributed also to this approach to simulating bolt tightening, as well as the assumed 419 isotropic material properties for the bolt based on tensile tests. Construction imperfections of the 420 experimental test setup may have also impacted both the slip and peak loads. The measured slip 421 load of Scenario 1 may have been especially impacted by any construction imperfections as such 422 imperfections may have imparted moment in a scenario for which only axial load was considered 423 in the FE model. 424

The FE models predicted a higher stiffness than the measured data, particularly for small displacements prior to slip. This difference can be attributed to play in the connection of the actuator to the moving member. The FE models for both Scenario 1 and Scenario 3 were able to accurately predict the deformed residual shape of the bolts (Figure 6A), with FE model for Scenario 1 predicting a double shear environment and the FE model for Scenario 3 predicting more of a single shear environment.

The FE models were able to show the loss in bolt tension, B due to the δ - and interferenceeffects in Scenario 3 compared to Scenario 1 (Figure 13). While Scenario 1 shows a constant bolt
tension along the length of the bolt, Scenario 3 indicates losses in bolt force toward the head of the
bolt due to the mechanisms shown in Figure 5. Likewise, bending, M in the bolt is also shown for
Scenario 3 in Figure 13, while no bending is shown for Scenario 1.

436 Analytical Predictions for Slip Load

453

Analytical predictions to capture the degradation in slip load were developed, incorporating the δ - and interference-effects. Specifically, a method to predict the bolt tension, T_b' was developed, where:

$$T_b' = T_b - F_\delta - F_h - F_c \tag{8}$$

where T_b is the bolt force for a straight and flush connection as given by design codes. The δ -effect 440 is considered by reducing the bolt force by a prediction, F_{δ} of the force to plastically deform the 441 plies into firm contact (Figure 5A). The flexural strains in the bolts from the δ -effect are ignored. 442 The interference-effect is considered by accounting for the force, F_h from the friction between 443 the plates and bolts due to bolt bending during installation (Figure 5B) and the force, F_c from the 444 friction from the catenary action of the bolt redirecting the bolt pretension around the corner of the 445 plate hole edge (Figure 5C). 446 An analytical approximation for F_{δ} considers the force required to deform the plates, assuming 447

that a full plastic hinge forms in TO at flange contact or the net section of TI: $F_{\delta} = max(M_{ppf}/l_{\delta 1}, M_{ppn}/l_{\delta 2})$, where M_{ppf} is the plastic moment capacity of the gross cross section of the plate $(F_u Z_x, M_{ppn}/l_{\delta 2})$, where F_u is the ultimate stress and Z_x is the plastic section modulus of the plate), M_{ppn} is the plastic moment capacity of net section of the plate, and $l_{\delta 1}$ and $l_{\delta 2}$ are defined in Figure 5A. This assumption is conservative as not all δ would result in a full plastic hinge forming.

The frictional force, F_h is calculated as: $F_h = \frac{2M_{pb}\mu}{t_m}$, where M_{pb} is the plastic moment capacity

of the bolt ($F_{ub}Z_{xb}$, where F_{ub} is the ultimate stress and Z_{xb} is the plastic section modulus of the bolt) and μ is the coefficient of friction. This assumes that plastic hinges form at the locations shown in Figure 5B.

The loss from catenary action, F_c is approximated as follows: $F_c = T_b \mu \sin \Theta$, where Θ is the angle over which the bolt must deform to accommodate the mis-aligned holes. Θ is calculated as: $\Theta = \tan^{-1}(\frac{e_b}{t_m})$

The predictions from this method are included as markers on Figure 10. Predictions are conservative and follow the same general trends as the measured data. For scenarios with low, but positive e_b , they become overly conservative due to the assumptions of fully plastic bolt and plate behavior. However this is a minor limitation to this predictive method.

These analytical predictions can also be compared to the FE predictions for tension in the bolt (Figure 13). Specifically, in the middle of the bolt, the FE model predicted a bolt tensile force of 19.0 kN (4.27 kips) for Scenario 1 and 14.3 kN (3.21 kips) for Scenario 3. The analytical predictions T'_b are 12.1 kN (2.72 kips) for Scenario 1 (i.e., no reduction) and 4.04 kN (0.908 kips) for Scenario 3. This further indicates that the analytical predictions are conservative compared to the FE predictions. This conservatism can be attributed to the assumption of fully plastic bolt and plate behavior in the analytical predictions.

471 CONCLUSIONS

479

This paper presented an experimental and numerical investigation of the behavior of adjustable bolted steel plate connections under axial load. The focus was on understanding the effect of the installation process and the connection geometry on the slip behavior and bolt shear failure mode of these connections. Based on these experimental and numerical studies, the following conclusions are made. Note that these conclusions may only be relevant to the specific scenarios studied in this research including ASTM A325 bolts (SAE Grade 5 equivalent), shallow member angles up to α = 17.5°, difference in ply angle, δ up to 2.5°, oversized plate holes, and long slot flange holes.

Measured slip loads for the adjustable bolted steel plate connections were found to be lower

than a comparable straight ($\alpha = 0^{\circ}$) and flush ($\delta = 0^{\circ}$) control scenario. This is due to the bolt installation process where bolts deform non-flush plates to contact with flanges and are being bent by contact with the plates. Both mechanisms degrade the clamping load.

- The measured slip load for scenarios where there is significant bolt deformation during installation ($e_b/d_b > 0$) during field installation is below the predicted design slip capacity. A mechanics-based method for predicting the slip load using geometric parameters has been developed.
- Measured peak loads for the adjustable bolted steel plate connection, for a failure mode
 of bolt shear, are found to be lower than a comparable straight and flush control scenario.
 While the connection is intended to be in double shear, the geometry of the connection
 (e_h/d_b greater than the minimum required elongation strain of the bolt) can result in only
 one shear plane being fully engaged, with partial or no engagement of the other.
- As the expected shear capacity was reduced, a design engineer should consider single shear capacity when e_h/d_b is greater than the minimum required elongation strain of the bolt from the applicable material specification, as well as a resistance factor.
- Bolt deformation, as classified by e_b/d_b and e_h/d_b ratios, has an impact on slip and bolt shear capacity, respectively, as defined above. A geometric limit $(e_b/d_b < 0.5)$ on the amount of permissible bolt deformation during bolt tightening has been developed to prevent bolt rupture during installation. High e_b/d_b values up to 0.3 were found to be acceptable with capacity reductions for slip and bolt shear due to the large strain to failure for the bolts in this research (measured elongation of 0.237).
- The ultimate capacity of the connection in compression is significantly lower than the connections in tension, as expected. The slip load was similar to that in tension.

Importantly, this research demonstrates that the slip and ultimate behavior of bent plate connections (common in skewed and curved girder cross frame connections for bridges and skewed beam connections in buildings) and misaligned and/or non-flush connections which are force-fit in the field may be degraded and not adequately represented in current design guidance. This is an

area for future research.

508 DATA AVAILABILITY STATEMENT

Some or all data, models, or code generated or used during the study are available from the corresponding author by request

511 ACKNOWLEDGMENTS

This material was based upon work supported by the National Science Foundation under Grant
No. CMMI-1351272. The support of Program Managers Drs. Kishor Mehta, Y. Grace Hsuan,
and Joy Pauschke is gratefully acknowledged. This research was also supported by the O. H.
Ammann Research Fellowship which was awarded to author Evan Gerbo. The authors are grateful
to Infra-metals and Steel Dynamics, Inc. for material donation and support.

517 REFERENCES

- 518 AASHTO (2012). AASHTO LRFD Bridge Construction Specifications. American Association of
- State Highway and Transportation Officials (AASHTO), 2012 Interim Revisions to 3rd Edition,
- Washington, D.C.
- 521 AASHTO (2014). AASHTO LRFD Bridge Design Specifications, Customary U.S. Units. American
- Association of State Highway and Transportation Officials (AASHTO), 7th Edition, with 2015
- and 2016 Interim Revisions, Washington, D.C.
- ABAQUS (2014). "ABAQUS/Standard Analysis User's Manual Version 6.14. Dassault Systemes,
- Waltham, MA.
- 526 AISC (2017). Steel Construction Maunal. American Institute of Steel Construction (AISC),
- 527 Chicago, IL, 15th edition.
- ASTM (2014a). "ASTM A325-14: Standard specification for structural bolts, steel, heat treated,
- 120/105 ksi minimum tensile strength." ASTM International. West Conshohocken, PA.
- 530 ASTM (2014b). "ASTM A36/A36M-14: Standard specification for carbon structural steel."
- ASTM International. West Conshohocken, PA.
- ASTM (2015). "ASTM F3125/F3125M-15a: Standard specification for high strength structural
- bolts, steel and alloy steel, heat treated, 120 ksi (830 mpa) and 150 ksi (1040 mpa) minimum
- tensile strength, inch and metric dimensions." ASTM International. West Conshohocken, PA.
- ASTM (2016). "ASTM F606/606M-16: Standard test methods for determining the mechanical
- properties of externally and internally threaded fasteners, washers, direct tension indicators, and
- rivets." ASTM International. West Conshohocken, PA.
- ASTM (2017a). "ASTM A370-17: Standard test methods and definitions for mechanical testing
- of steel products." ASTM International. West Conshohocken, PA.

- ASTM (2017b). "ASTM A6/A6M-17: Standard specification for general requirements for rolled structural steel bars, plates, shapes, and sheet piling." ASTM International. West Conshohocken,
- 542 PA.

553

- ASTM (2017c). "ASTM E111-17: Standard test method for young's modulus tangent modulus, and chord modulus." ASTM International. West Conshohocken, PA.
- ASTM (2017d). "ASTM E132-17 (reapproved 2010): Standard test method for poisson's ratio at room temperature." ASTM International. West Conshohocken, PA.
- ASTM (2018). "ASTM F436/F436M-18a: Standard specification for hardened steel washers inch and metric dimensions." ASTM International. West Conshohocken, PA.
- Gerbo, E. J., Thrall, A. P., Smith, B. J., and Zoli, T. P. (2016). "Full-field measurement of residual strains in cold bent steel plates." *Journal of Constructional Steel Research*, 127, 187–203.
- Gerbo, E. J., Thrall, A. P., and Zoli, T. P. (2019a). "Adjustable bolted steel plate connection:

 Measured behavior of bolts during field installation and numerical parametric investigation."

Journal of Structural Engineering, In press.

- Gerbo, E. J., Wang, Y., Tumbeva, M. D., Thrall, A. P., Smith, B. J., and Zoli, T. P. (2018). "Behavior
 of an adjustable bolted steel plate connection during field installation." *Journal of Structural* Engineering, 144(3), 04017223.
- Gerbo, E. J., Wang, Y., Tumbeva, M. D., Thrall, A. P., Smith, B. J., and Zoli, T. P. (2019b). "Closure
 to 'Behavior of an Adjustable Bolted Steel Plate Connection during Field Installation' by Evan
 J. Gerbo, Yao Wang, Mirela D. Tumbeva, Ashley P. Thrall, Brian J. Smith, and Theodore P.
 Zoli." Journal of Structural Engineering, 145(3), 07018015.
- Kulak, G. L., Fisher, J. W., and Struik, J. H. A. (2001). *Guide to Design Criteria for Bolted and*Riveted Joints. American Institute of Steel Construction, 2nd Edition, Chicago, I.L.

- Research Council on Structural Connections (2014). "Specifications for Structural Joints Using
- High-Strength Bolts.
- ⁵⁶⁵ SAE (2014). "SAE J429: Mechanical and material requirements for externally threaded fasteners."
- SAE International. Warrendale, PA.

567 List of Tables

568	1	Experimentally tested connection parameters. See Figure 1	25
569	2	Measured material properties. E = elastic modulus, F_y = yield strength, F_u =	
570		ultimate strength, ν = Poisson's ratio, Std. Dev. = standard deviation, COV =	
571		coefficient of variation.	26

Scen.	γ	α	δ	Other Parameters	e_b	Slip Load	e_h	Peak Load
	(deg.)	(deg.)	(deg.)		(mm)	(kN)	(mm)	(kN)
1	0	0	0	Control	-1.59	29.0	0	154
2	0	0	0	Standard holes	-0.794	25.1	0	149
3a	10	12.5	2.5	Benchmark a	1.74	14.0	3.33	91.7
3b	10	12.5	2.5	Benchmark b	1.74	11.0	3.33	87.6
3c	10	12.5	2.5	Benchmark c	1.74	12.2	3.33	92.1
4	12.5	12.5	0		1.41	15.9	3.00	91.8
5	15	12.5	-2.5		1.37	16.6	2.95	95.9
6	10	12.5	2.5	Beveled washers	1.74	6.3	3.33	79.8
7	10	12.5	2.5	Increased tightening	1.74	-	3.33	-
8	10	12.5	2.5	Compression	1.74	12.6	3.33	35.8
9	0	2.5	2.5		-0.961	23.4	0.627	147
10	5	5	0		-0.404	26.4	1.18	114
11	5	7.5	2.5		0.376	23.0	1.96	90.7
12	5	2.5	-2.5		-1.01	24.4	0.578	150
13	10	10	0		0.797	20.2	2.38	87.6
14	10	7.5	-2.5		0.165	26.7	1.75	106
15	15	15	0		2.04	17.9	3.62	85.2
16	15	17.5	2.5		3.16	-	4.75	-

TABLE 1. Experimentally tested connection parameters. See Figure 1.

26

Component	Property	E	F_y	F_u	ν
		(GPa)	(Mpa)	(Mpa)	
	Mean	218	325	483	0.281
Plate	Std. Dev.	7.01	2.54	1.04	0.00250
	COV %	3.21	0.784	0.215	0.215
	Mean	226	872	938	-
Bolt	Std. Dev.	8.41	23.4	10.9	-
	COV %	3.73	2.69	1.17	-

TABLE 2. Measured material properties. E = elastic modulus, F_y = yield strength, F_u = ultimate strength, ν = Poisson's ratio, Std. Dev. = standard deviation, COV = coefficient of variation.

572 List of Figures

573	1	Adjustable bolted steel plate connection including: (A) prefabrication via a press	
574		brake, (B) isometric view of tightened connection, (C) elevation view of untight-	
575		ened connection, (D) final tightened connection, (E) top flange bolt numbering, and	
576		(F) bottom flange bolt numbering. Image (A) reprinted from Journal of Construc-	
577		tional Steel Research, 127, EJ Gerbo, AP Thrall, BJ Smith, and TP Zoli, Full-field	
578		Measurement of Residual Strains in Cold Bent Steel Plates, 187-203, 2016, with	
579		permission from Elsevier. Images (B-F) adapted from Gerbo et al. (2019a) ©ASCE.	29
580	2	Experimental test setup: (A) Scenario 1 during bolt tightening, (B) Scenario 1 with	
581		actuator applying load, (C) rendering of Scenario 1, (D) Scenario 3 during bolt	
582		tightening, (E) Scenario 3 with actuator applying load, (F) rendering of Scenario 3,	
583		(G) detailed view of Scenario 3, (H) instrumentation, (I) DIC measurement locations.	30
584	3	FE numerical model	31
585	4	Measured actuator force, F , versus actuator displacement, Δ behavior for straight	
586		and flush control tests and the adjustable bolted steel plate connection. Red indi-	
587		cates flush (δ =0), green indicates $+\delta$, and blue indicates $-\delta$	32
588	5	Mechanisms for degradation in slip and bolt shear capacities: (A) δ -effect reducing	
589		slip capacity, (B) interference-effect reducing slip capacity: friction from contact	
590		due to plate bending, (C) interference-effect reducing slip capacity: catenary action	
591		friction, (D) connection geometry leading to reduced bolt shear capacity	33
592	6	Residual (i.e., after testing was completed) bolt deformations: (A) measured and	
593		predicted full-field lateral, x displacements and (B) measured lateral location of	
594		centerlines along the bolt axis, y	34
595	7	Measured slip along faying surfaces	35
596	8	Effect of direction of loading: Measured actuator force, F , versus actuator dis-	
597		placement, Δ behavior in tension and compression	36

598	9	Effect of varying plate and member angles: Measured actuator force, F, versus	
599		actuator displacement, Δ behavior. Red indicates flush (δ =0), green indicates $+\delta$,	
600		and blue indicates $-\delta$	37
601	10	Normalized measured slip loads, F_s compared to normalized analytical prediction	
602		of bolt deformation, e_b . Red indicates flush (δ =0), green indicates $+\delta$, and blue	
603		indicates $-\delta$. Circles indicate predicted values considering mechanics-based re-	
604		ductions	38
605	11	Normalized measured peaks loads, \mathcal{F}_p compared to normalized analytical predic-	
606		tion of offset between the plate holes, e_h . Red indicates flush (δ =0), green indicate	
607		$+\delta$, and blue indicates $-\delta$	39
608	12	Normalized measured DIC residual bolt shear deformations, s compared to nor-	
609		malized analytical prediction of offset between the plate holes, e_h for (A) top flange	
610		bolts and (B) bottom flange bolts. Red indicates flush (δ =0), green indicates $+\delta$,	
611		and blue indicates $-\delta$	40
612	13	FE predictions of the axial force, B and moment, M in the bolt, along the axis of	
613		the bolt, <i>y</i> after field installation.	41

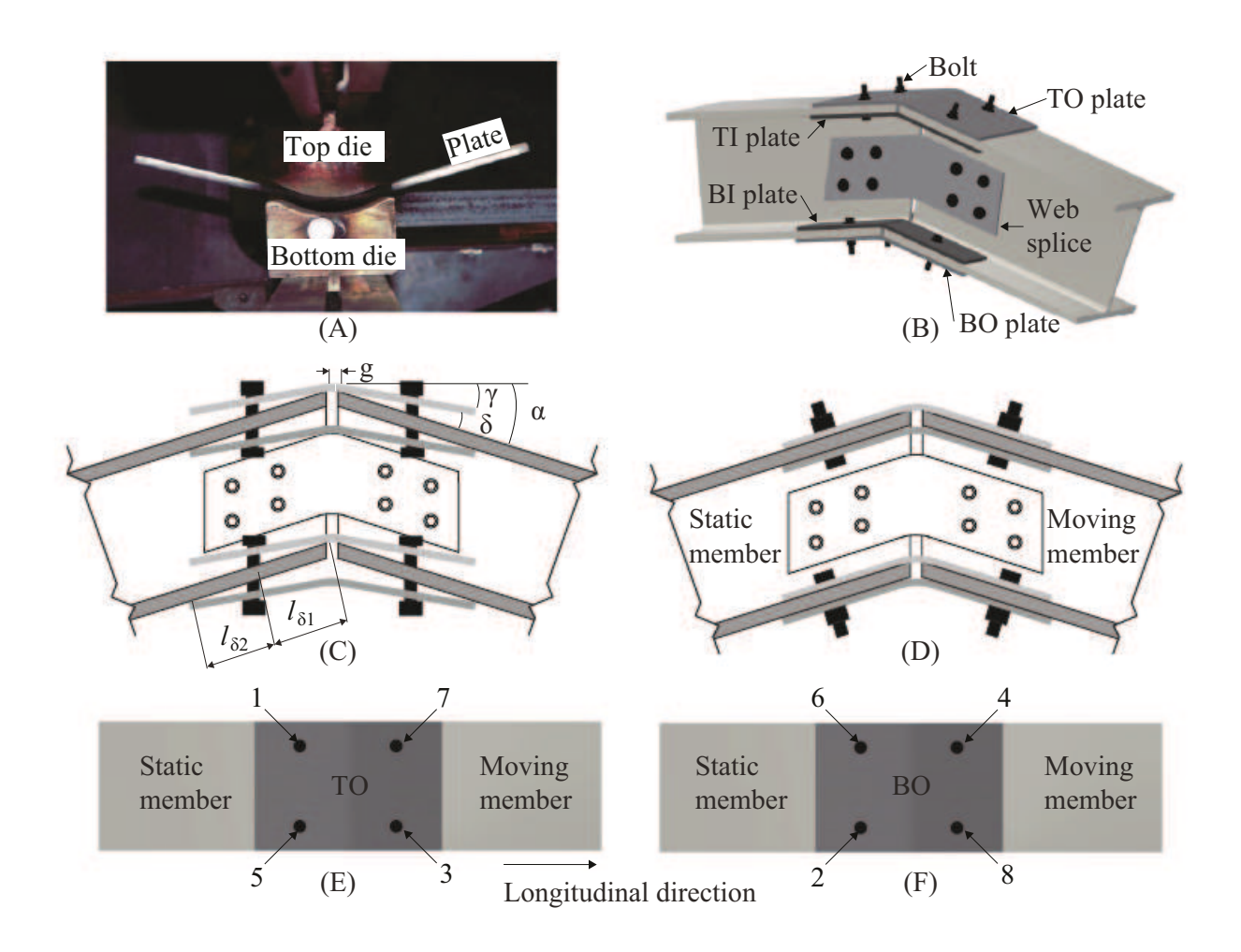


FIG. 1. Adjustable bolted steel plate connection including: (A) prefabrication via a press brake, (B) isometric view of tightened connection, (C) elevation view of untightened connection, (D) final tightened connection, (E) top flange bolt numbering, and (F) bottom flange bolt numbering. Image (A) reprinted from Journal of Constructional Steel Research, 127, EJ Gerbo, AP Thrall, BJ Smith, and TP Zoli, Full-field Measurement of Residual Strains in Cold Bent Steel Plates, 187-203, 2016, with permission from Elsevier. Images (B-F) adapted from Gerbo et al. (2019a) ©ASCE.

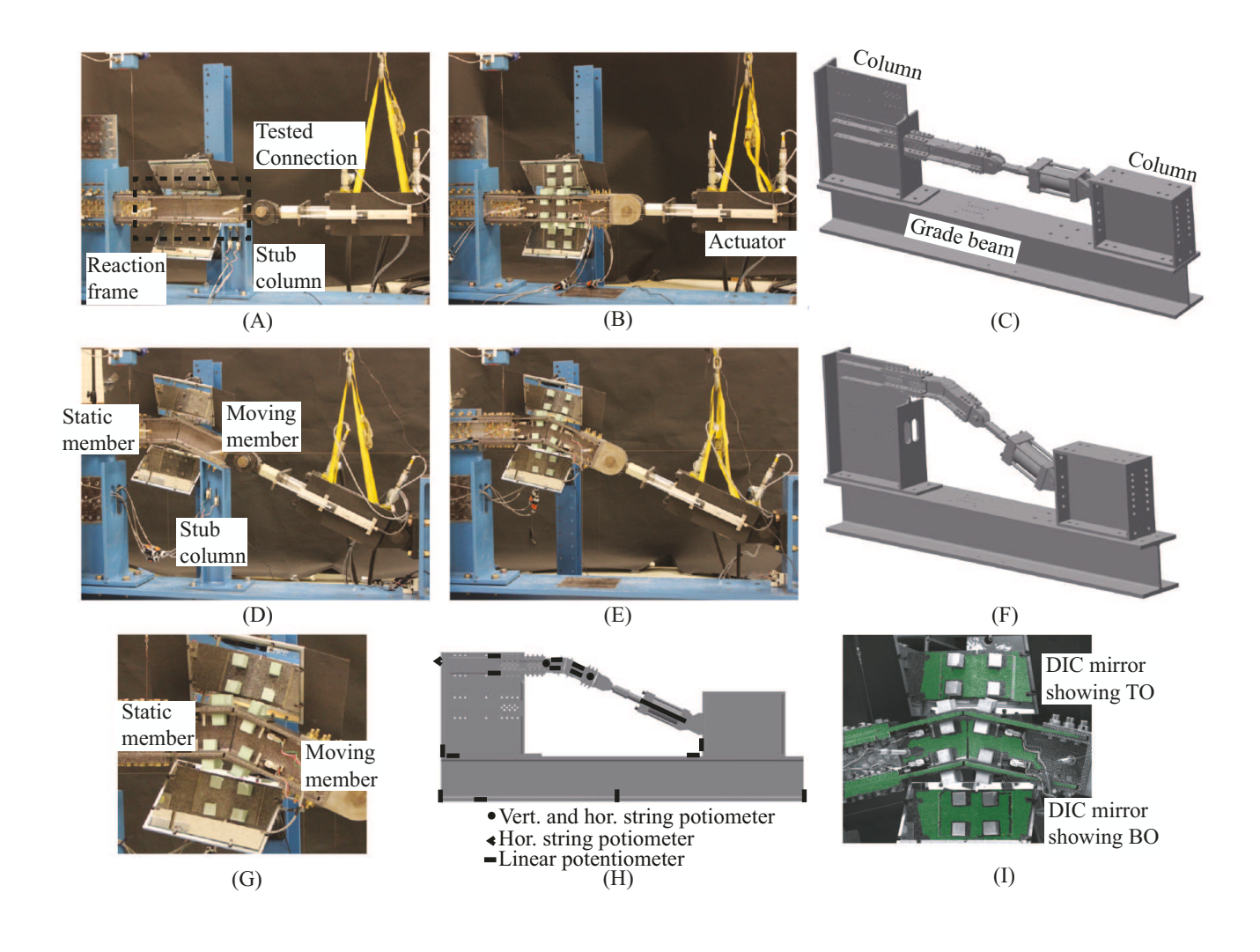


FIG. 2. Experimental test setup: (A) Scenario 1 during bolt tightening, (B) Scenario 1 with actuator applying load, (C) rendering of Scenario 1, (D) Scenario 3 during bolt tightening, (E) Scenario 3 with actuator applying load, (F) rendering of Scenario 3, (G) detailed view of Scenario 3, (H) instrumentation, (I) DIC measurement locations.

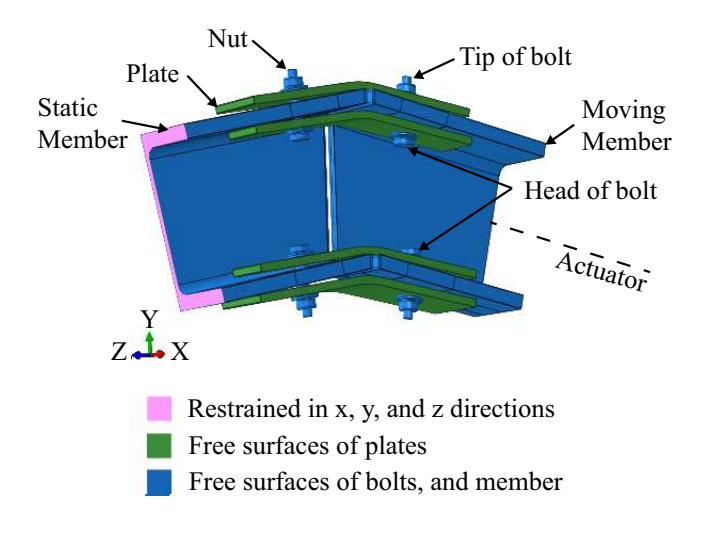


FIG. 3. FE numerical model.

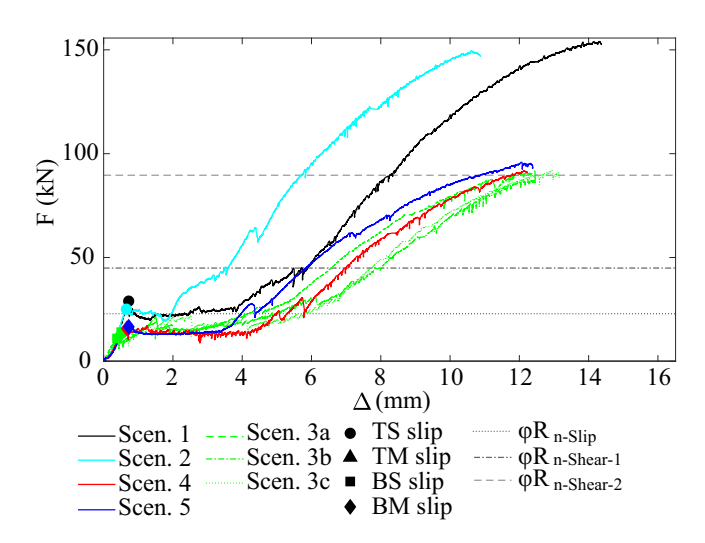


FIG. 4. Measured actuator force, F, versus actuator displacement, Δ behavior for straight and flush control tests and the adjustable bolted steel plate connection. Red indicates flush (δ =0), green indicates $+\delta$, and blue indicates $-\delta$.

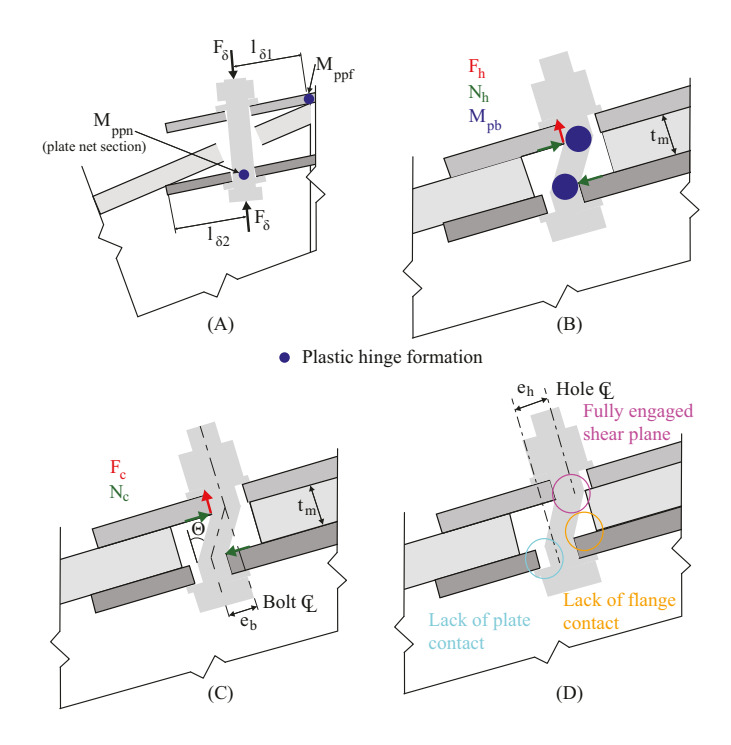


FIG. 5. Mechanisms for degradation in slip and bolt shear capacities: (A) δ -effect reducing slip capacity, (B) interference-effect reducing slip capacity: friction from contact due to plate bending, (C) interference-effect reducing slip capacity: catenary action friction, (D) connection geometry leading to reduced bolt shear capacity.

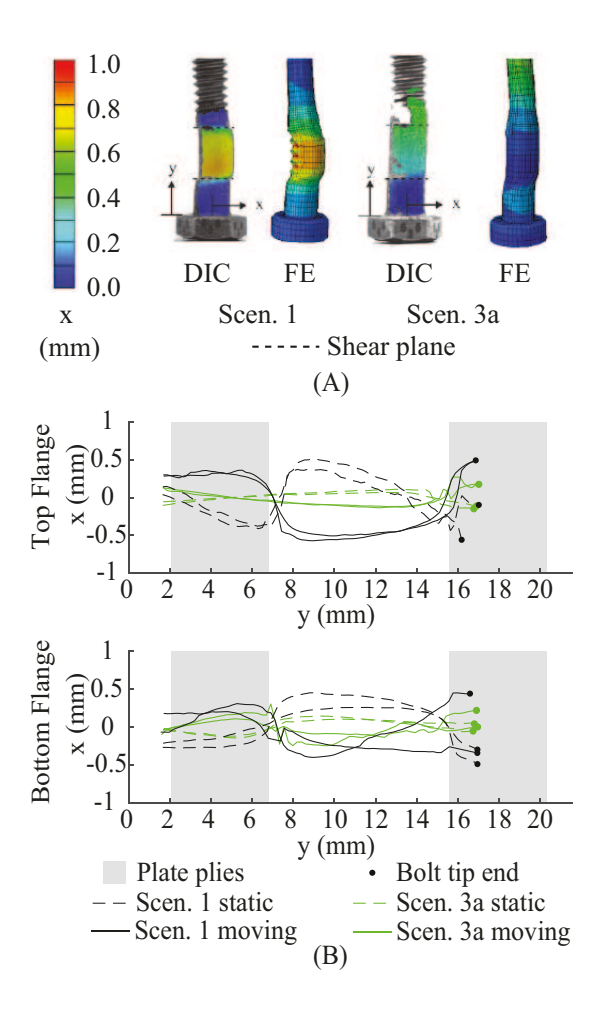


FIG. 6. Residual (i.e., after testing was completed) bolt deformations: (A) measured and predicted full-field lateral, x displacements and (B) measured lateral location of centerlines along the bolt axis, y.

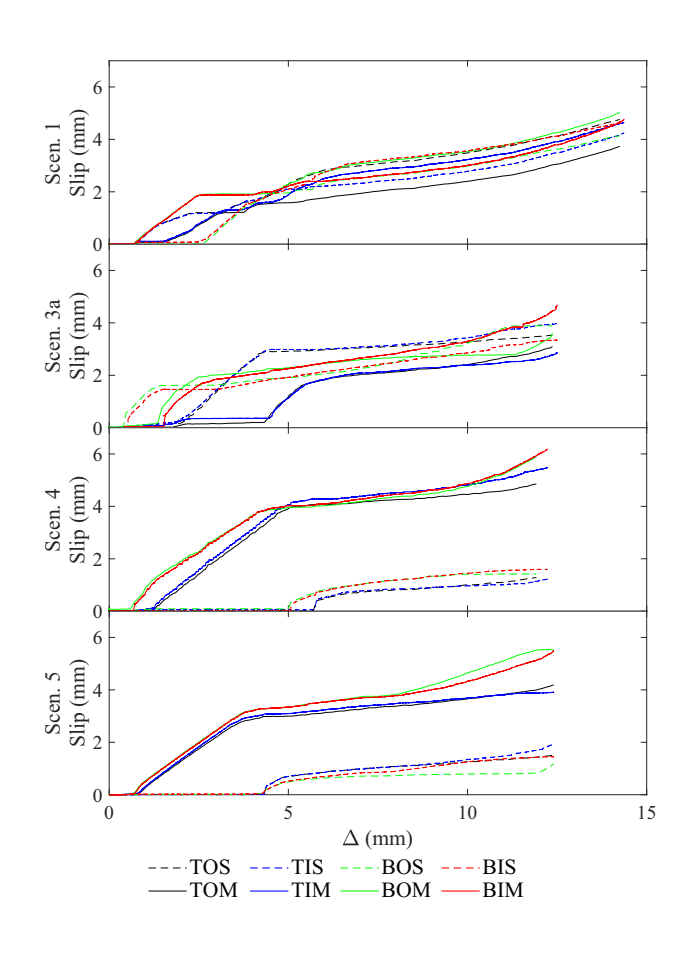


FIG. 7. Measured slip along faying surfaces.

36

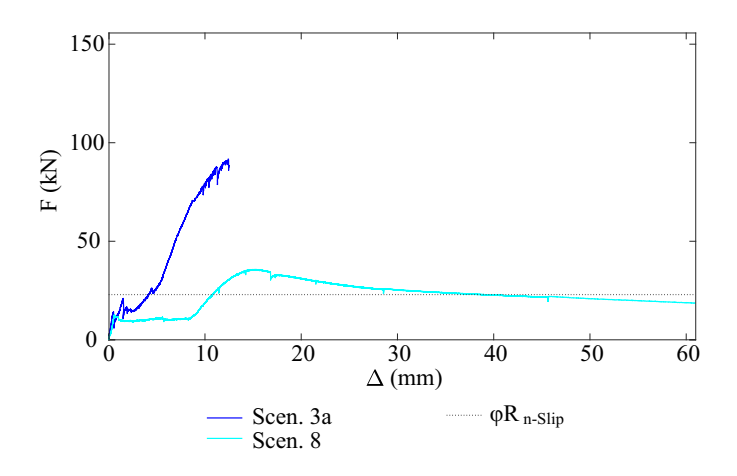


FIG. 8. Effect of direction of loading: Measured actuator force, ${\cal F}$, versus actuator displacement, Δ behavior in tension and compression.

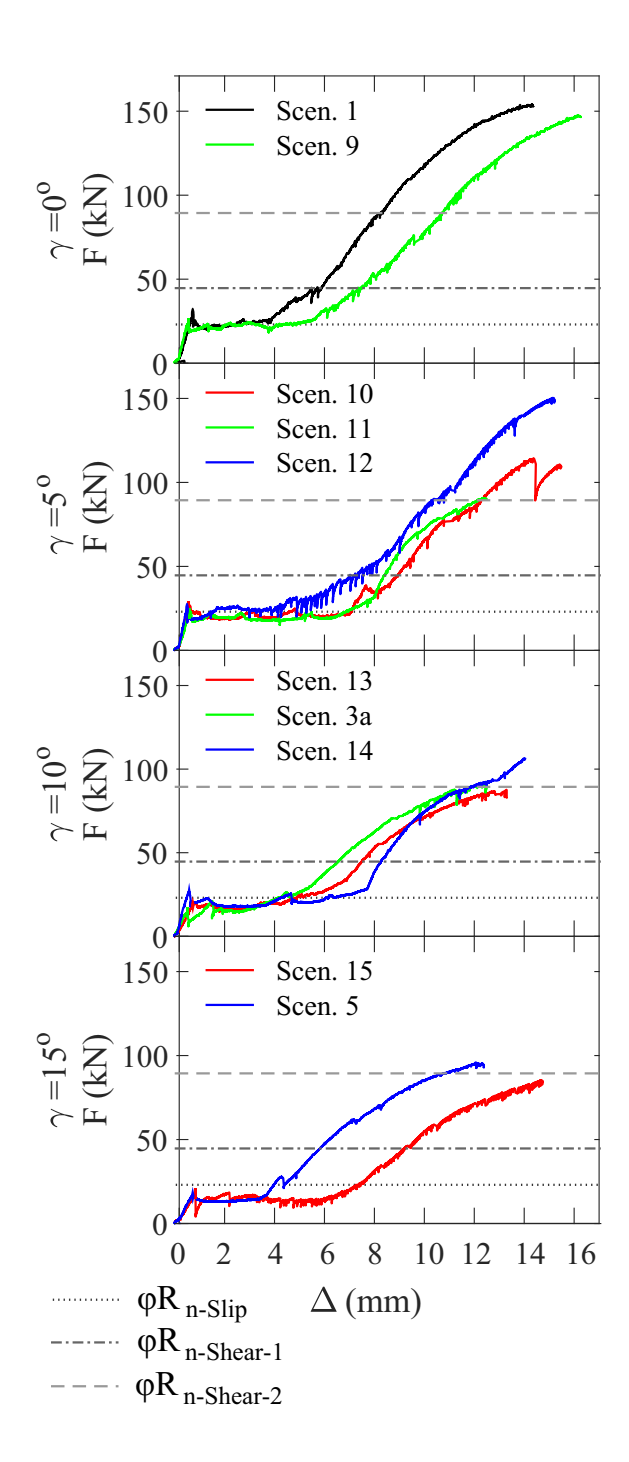
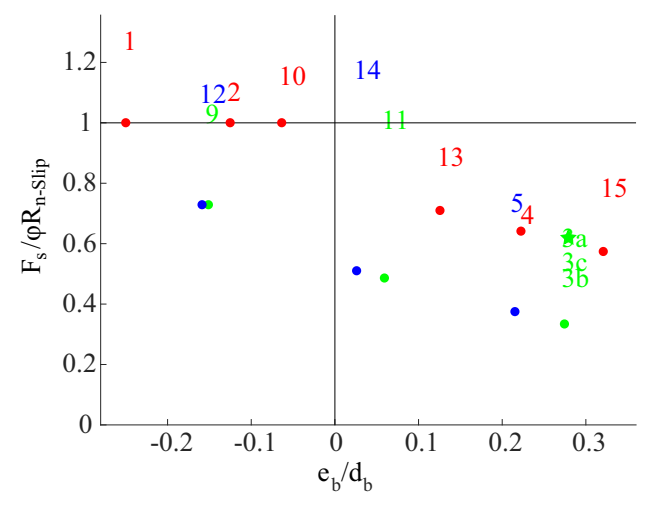


FIG. 9. Effect of varying plate and member angles: Measured actuator force, F, versus actuator displacement, Δ behavior. Red indicates flush (δ =0), green indicates $+\delta$, and blue indicates $-\delta$.



- # Measured, number indicates scenario
- Analytical prediction associated with scenario
- ★ FE prediction

FIG. 10. Normalized measured slip loads, F_s compared to normalized analytical prediction of bolt deformation, e_b . Red indicates flush (δ =0), green indicates $+\delta$, and blue indicates $-\delta$. Circles indicate predicted values considering mechanics-based reductions.

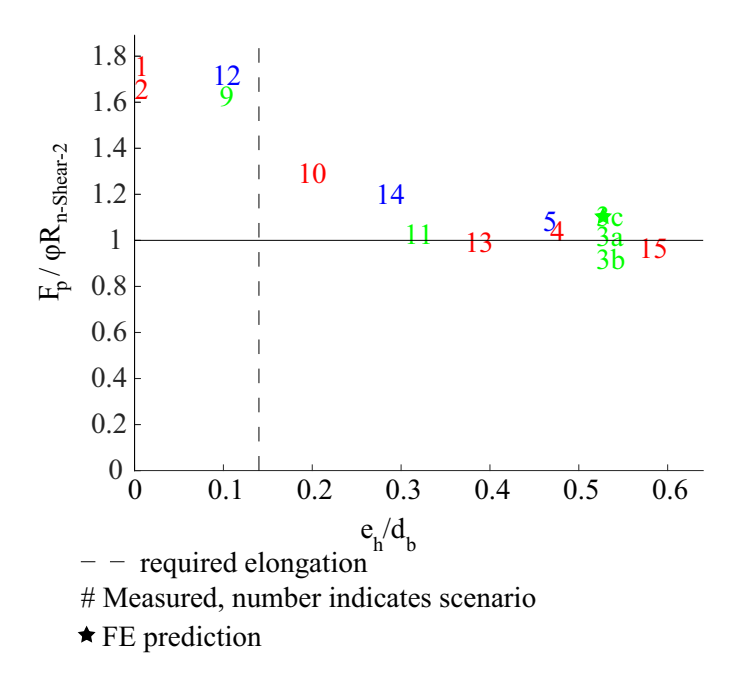


FIG. 11. Normalized measured peaks loads, F_p compared to normalized analytical prediction of offset between the plate holes, e_h . Red indicates flush (δ =0), green indicate $+\delta$, and blue indicates $-\delta$.

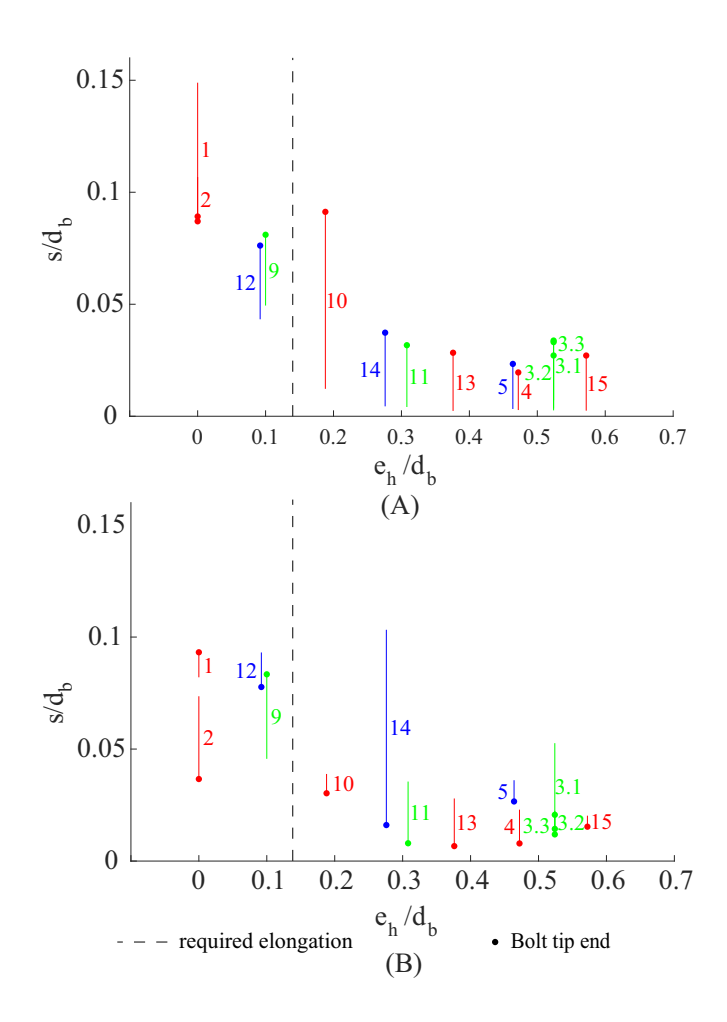


FIG. 12. Normalized measured DIC residual bolt shear deformations, s compared to normalized analytical prediction of offset between the plate holes, e_h for (A) top flange bolts and (B) bottom flange bolts. Red indicates flush (δ =0), green indicates $+\delta$, and blue indicates $-\delta$.

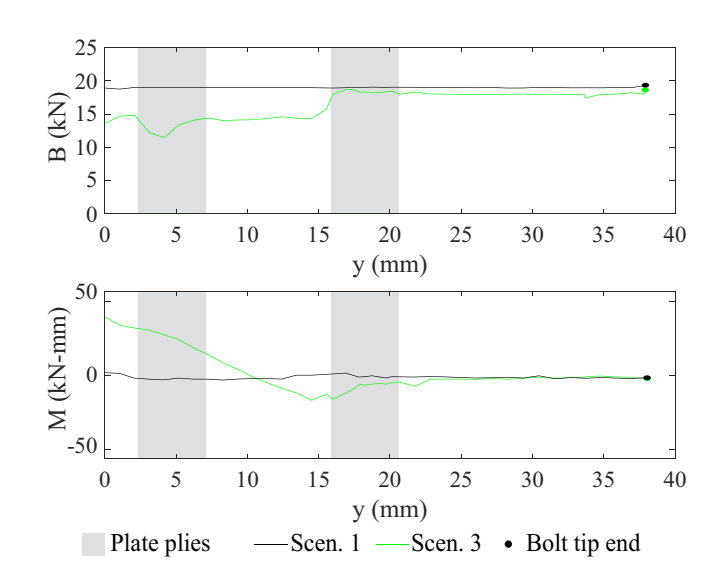


FIG. 13. FE predictions of the axial force, B and moment, M in the bolt, along the axis of the bolt, y after field installation.